IEEE Photonics Journal
An IEEE Photonics Society Publication

Open Access

Thermo-Optically Controlled Vertical Waveguide Directional Couplers for Mode-Selective Switching

Volume 10, Number 6, December 2018

Quandong Huang
Kin Seng Chiang, ***Member, IEEE***
Wei Jin

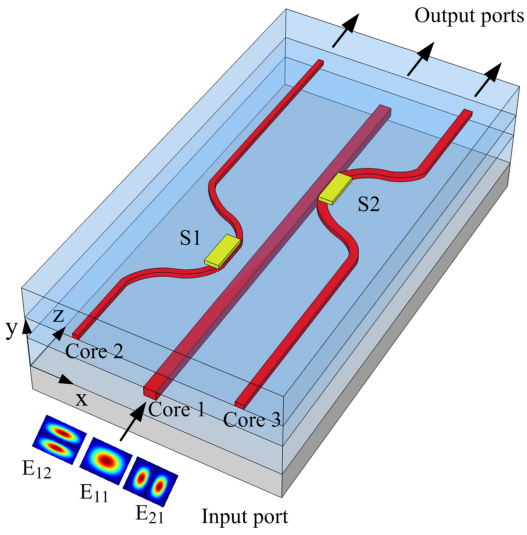

DOI: 10.1109/JPHOT.2018.2882467
1943-0655 © 2018 IEEE

IEEE photonics SOCIETY

IEEE

Thermo-Optically Controlled Vertical Waveguide Directional Couplers for Mode-Selective Switching

Quandong Huang, Kin Seng Chiang, *Member, IEEE*, and Wei Jin

Department of Electronic Engineering, City University of Hong Kong, Kowloon Hong Kong, SAR

DOI:10.1109/JPHOT.2018.2882467

Manuscript received October 30, 2018; accepted November 16, 2018. Date of publication November 20, 2018; date of current version December 4, 2018. This work was supported by the Research Grants Council of the Hong Kong Special Administrative Region, China, under Project CityU 11253316.
Corresponding author: K. S. Chiang (e-mail: eeksc@cityu.edu.hk).

Abstract: We propose a three-dimensional waveguide structure for the realization of mode-selective switches, where the high-order spatial modes of a few-mode waveguide can be switched to various single-mode waveguides with thermo-optically controlled vertical asymmetrical directional couplers. To demonstrate the idea, we design and fabricate two specific devices with a polymer material for a waveguide that supports three spatial modes. The two devices differ in the application of the thermo-optic effect to deactivate or activate the directional couplers. For one device, the switching powers measured at the wavelength 1550 nm are lower than 20.6 mW and the switching times are shorter than 4.4 ms. The extinction ratios are higher than 15.6 dB across the C-band measured at fixed switching powers. For the other device, the switching powers measured at 1550 nm are lower than 22.6 mW, the switching times are shorter than 2.9 ms, and the extinction ratios are higher than 14.1 dB in the C-band. The performances of the devices are weakly sensitive to the polarization state of light. Our proposed mode-selective switches, which have a scalable configuration and require low power consumption, could be developed into various active mode-controlling devices for applications in reconfigurable mode-division-multiplexing networks.

Index Terms: Integrated optics, mode-division multiplexing, optical switching device, optical waveguide coupler, polymer waveguide, thermo-optic effect.

1. Introduction

Mode-division multiplexing (MDM), where different spatial modes or mode groups in a few-mode fiber carry different signal channels, is a promising technology to expand the limited transmission capacity of a single-mode fiber [1]–[4]. Mode (de)multiplexers for spatially combining or separating the modes of a few-mode fiber are the key components in MDM systems and have been demonstrated with different waveguide structures and material systems (e.g., [5]–[17]). Planar waveguide structures, such as horizontal directional couplers [5] and multimode interferometers [6], however, can only (de)multiplex spatial modes that have the same symmetry in the vertical direction (e.g., the LP_{01} and the LP_{11a} mode). They cannot (de)multiplex spatial modes that have opposite symmetries in the vertical direction (e.g., the LP_{01} and the LP_{11b} mode). As such, these devices pose significant limitation on their application in fiber-based MDM systems, where the modes can have different symmetries in both the horizontal and the vertical direction. The mode-symmetry issue

in the realization of mode-selective couplers has been analyzed in detail with fiber couplers [18]. One approach to solving this problem is to use a mode rotator to change the symmetry property of the problematic mode (e.g., to convert the LP_{11b} mode into the LP_{11a} mode) [7], [8]. The mode rotator can be a carefully trenched waveguide [7] or an asymmetric long-period waveguide grating [8]. The other approach is to use three-dimensional (3D) structures [9]–[17], such as fiber lanterns [9], combined horizontal and vertical directional couplers [10]–[14], all vertical directional couplers [15], 3D waveguide branches [16], and non-planar directional couplers [17]. As multilayer structures can be easily formed with polymer material, many of these 3D mode (de)multiplexers [12]–[17] are implemented with polymer waveguides. All the aforementioned devices are passive devices. For a reconfigurable MDM-based network that involves switching and routing of mode channels, however, active devices that can dynamically combine/separate the modes into/from the bus fiber are required. This paper reports mode spatial switches based on a 3D waveguide structure.

In general, a mode spatial switch can be implemented by connecting a passive mode demultiplexer to a single-mode switch matrix and such a bulk switch has been demonstrated for the operation of the LP_{01}, LP_{11a}, and LP_{11b} modes with $LiNbO_3$ single-mode waveguide switches [19]. To improve compactness and stability, a number of integrated thermo-optic (TO) mode spatial switches have been reported, which exploit a wide range of waveguide structures and their combinations, such as directional coupler [20], [21], Mach-Zehnder interferometer [22]–[24], multimode interference waveguide (MMI) [24], microring resonator [25], waveguide branch [22], [26], and long-period grating [26]. These integrated mode spatial switches, however, are planar structures and cannot process modes with opposite symmetries in the vertical direction. Indeed, they have been demonstrated only for the operation of vertically symmetric modes. Recently, we have proposed a TO mode spatial switch based on the structure of two cascaded vertical asymmetric directional couplers and presented preliminary results on a specific design [27]. The device allows the LP_{11a} and LP_{11b} modes of a three-mode waveguide to be switched into two single-mode waveguides, respectively, by applying the TO effect to deactivate the two directional couplers, respectively [27]. In this paper, we present detailed results on the design, the fabrication, and the characterization of two devices, which differ in the application of the TO effect to deactivate or activate the vertical directional couplers. Both devices are fabricated with the same polymer material system. The device based on deactivating the directional couplers shows a switching power lower than 20.6 mW and a switching time shorter than 4.4 ms at the wavelength 1550 nm with extinction ratios higher than 15.6 dB across the C-band measured at fixed switching powers. The device based on activating the directional couplers shows a switching power lower than 22.6 mW and a switching time shorter than 2.9 ms at 1550 nm with extinction ratios higher than 14.1 dB across the C-band. The two devices have comparable performances, which are weakly sensitive to the polarization of light. Our proposed structure is scalable, as the number of switchable modes can be increased by increasing the number of vertical directional couplers. In fact, we have recently demonstrated a passive six-mode (de)multiplexer with five cascaded vertical directional couplers designed for operation in the C-band [15]. Our devices could be used as mode-adding switches in MDM systems, and also as mode-dropping switches in MIMO-free systems based on elliptical-core few-mode fibers [28]–[32], where mode couplings among the spatial modes are weak.

2. Design of TO Mode Spatial Switches

The structure of our proposed device is shown in Fig. 1, which consists of two cascaded vertical asymmetric directional couplers with a few-mode waveguide core (FMC) (Core 1) located in the lower layer and two single-mode waveguide cores (SMCs) (Core 2 and Core 3) located in the upper layer. All the cores are surrounded with the same cladding material. Two electrode heaters are deposited on the surface of the upper cladding to control the coupling efficiencies of the two directional couplers, respectively, which thus function as two TO switches (S1 and S2). In addition to design flexibility, the use of a vertical coupler allows a much larger temperature difference between the two cores produced by the electrode heater, which can lead to a lower switching power, compared with the use of a conventional horizontal directional coupler [19]. The FMC

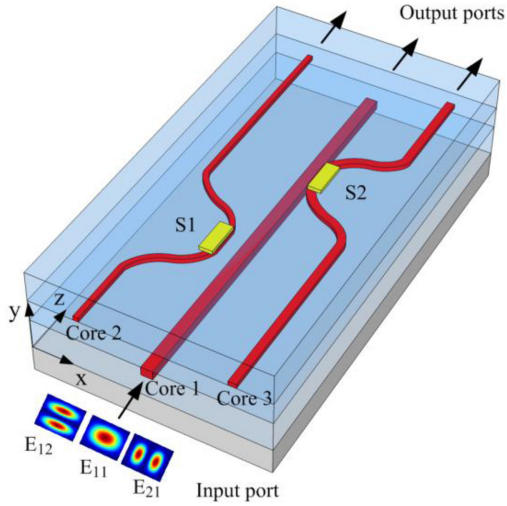

Fig. 1. Structure of the proposed spatial switch, which consists of two cascaded TO-controlled vertical directional couplers.

supports three spatial modes, the E_{11}, E_{21}, and E_{12} modes, which correspond to the LP_{01}, LP_{11a}, and LP_{11b} modes of a few-mode fiber, respectively [33]. The mode patterns are also shown in Fig. 1. We should note that each spatial mode consists of two polarizations: the transverse-electric (TE) polarization for the mode with the major electric-field component parallel to the waveguide surface and the transverse-magnetic (TM) polarization for the mode with the major electric-field component perpendicular to the waveguide surface. When the refractive-index difference between the cores and the cladding is small, as in our case, the two polarization modes are almost degenerate.

We present two designs, Design I and Design II, which differ in the use of the TO effect to deactivate or activate the directional couplers. We analyze the modes of the devices with a full-vector finite-element method (COMSOL). The refractive indices of the core and the cladding material used in the design work are 1.569 and 1.559, respectively, which are the refractive indices of the polymer materials used in our fabrication work.

2.1 Design I

In Design I, the core sizes are so designed that they satisfy the phase-matching conditions when both heater switches are off, i.e., the effective indices of the E_{11} modes in Core 2 and Core 3 match those of the E_{12} and E_{21} modes in Core 1, respectively. Here, we present a typical design. The dimensions of the two directional couplers are shown in Figs. 2(a) and (b), respectively. The heights of the FMC and the SMCs are fixed at 7.0 and 4.0 μm, respectively, and the vertical gap spacing between the FMC and the SMCs is 3.0 μm. The centers of Core 2 and Core 3 are offset from that of Core 1 by 8.6 and 7.3 μm, respectively. The widths of Core 1, Core 2, and Core 3 are 10.0, 3.0, and 5.4 μm, respectively. These waveguide parameters ensure that the effective indices of the E_{11} modes in Core 2 and Core 3 match those of the E_{12} and E_{21} modes in Core 1, respectively, at the wavelength 1550 nm, as shown in Fig. 2(c) for the *x*-polarization. The results for the *y*-polarization are almost the same and, therefore, not shown in the figure. The lengths of the couplers required for maximum power transfer are determined with a 3D finite-difference beam propagation method (3DFD-BPM, RSoft). S-bends are applied to separate the SMCs and the FMC at both ends. The coupling lengths of the first and the second coupler are 3.75 and 3.80 mm, respectively. We ignore propagation loss and material dispersion in the simulation and the performance of the device is optimized at the wavelength 1550 nm. With this design, when both switches are turned off, the E_{12} and E_{21} modes launched into Core 1 are completely coupled to the E_{11} modes in Core 2 and Core 3, respectively, while the E_{11} mode launched into Core 1 stays in Core 1. When both switches

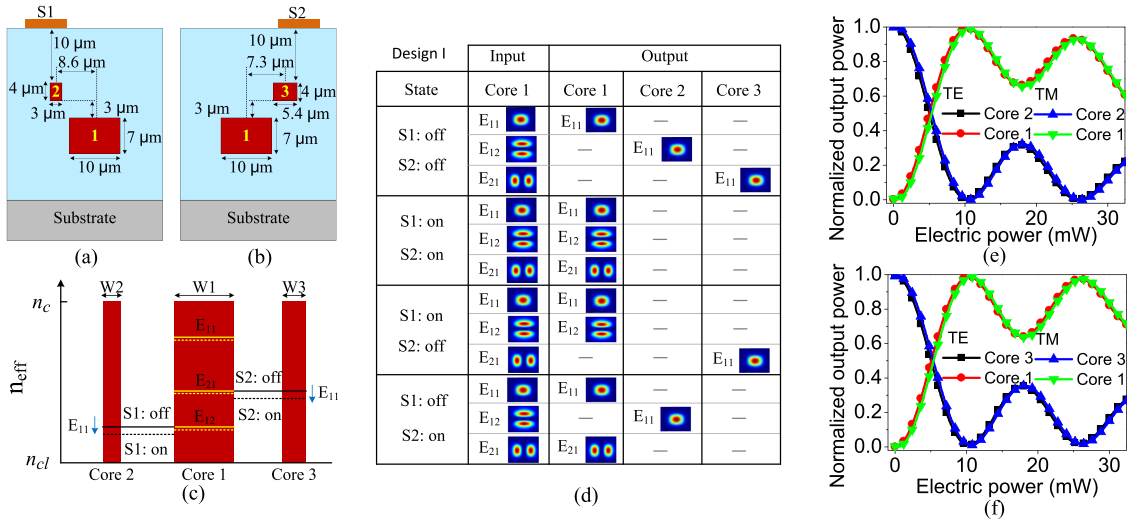

Fig. 2. Design I: dimensions of (a) the first and (b) the second directional coupler; (c) the phase-matching conditions for the two directional couplers, where w1, w2, and w3 denote the widths of Core 1, Core 2, and Core 3, respectively, and n_{eff} denotes the effective index; (d) switching functions of the device; and variations of the normalized output powers with the applied electric power for (e) S1 and (f) S2.

are turned on, because of the TO effect, the refractive indices of all the cores decrease but those of Core 2 and Core 3 decrease more. As a result, the phase-matching conditions are no longer satisfied and all the modes launched into Core 1 stay in Core 1. In other words, the TO effect deactivates the couplers. When one of the switches is turned on, only one of the high-order modes is switched. The functions of this switch are summarized in Fig. 2(d). To estimate the switching powers of the design, we apply the built-in electrode-heater model in the 3DFD-BPM and calculate the variations of the normalized output light powers with the applied electric power for the two switches, where the TO coefficient of the polymer material is taken to be -8.0×10^{-5} /°C. The results for S1 and S2 obtained at 1550 nm are shown in Figs. 2(e) and (f), respectively. The electric powers required for S1 and S2 are estimated to be 10.4 and 10.6 mW, respectively, which are polarization-insensitive. These electric powers are set for the "on" states of S1 and S2.

The coupling strength of each directional coupler is characterized by the coupling ratio, which is defined as the output optical power from one port over the total output power from both ports. Assuming that only the E_{mn} mode is launched into Core 1, the coupling ratios of the two directional couplers with the corresponding switch turned off and on, denoted as $CR_{mn|OFF}$ and $CR_{mn|ON}$, respectively, with $mn = 12$ for the first coupler and $mn = 21$ for the second coupler, are given by

$$CR_{mn|OFF} = \frac{P_{mn|OFF}}{P_{total|OFF}} \text{ and } CR_{mn|ON} = \frac{P_{mn|ON}}{P_{total|ON}}, \tag{1}$$

where $P_{mn|OFF}$ and $P_{mn|ON}$ are the output powers from the SMC intended for the E_{mn} mode, i.e., Core 2 for $mn = 12$ and Core 3 for $mn = 21$, when the switch of concern is turned off and on, respectively, and $P_{total|OFF}$ and $P_{total|ON}$ are the total output powers from the two ports of the directional coupler when the switch is turned off and on, respectively. The calculated coupling ratios for the two directional couplers are shown in Figs. 3(a) and (b), respectively. In the C-band, $CR_{12|OFF}$ and $CR_{21|OFF}$ are higher than 96.9% (93.9%) and 97.9% (96.8%) for the TE (TM) polarization, respectively, while $CR_{12|ON}$ and $CR_{21|ON}$ are lower than 3.1% (6.1%) and 2.1% (3.2%) for the TE (TM) polarization, respectively.

The effectiveness of a switch is characterized by the extinction ratio (in dB), which is the ratio of the output powers from the desired port of the directional coupler obtained at the "off" and "on" states of the switch, respectively. The extinction ratios of S1 and S2, denoted as ER_{mn} with

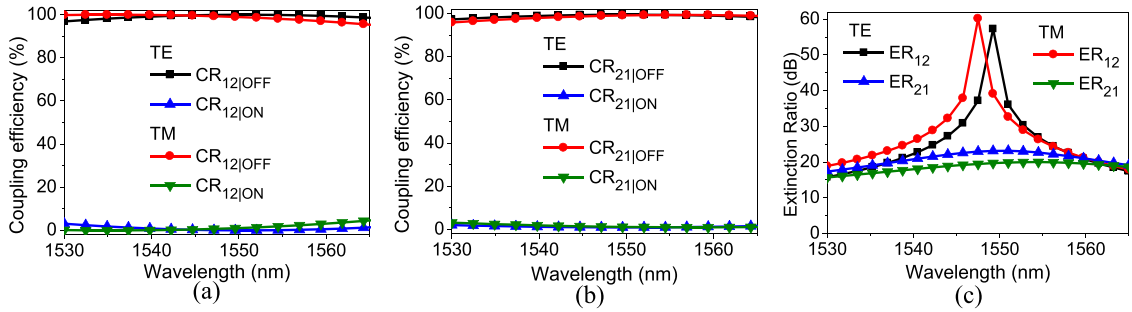

Fig. 3. Design I: coupling ratios for (a) the first and (b) the second directional coupler when the corresponding switches are turned off or on; and (c) the extinction ratios of S1 and S2.

$mn = 12$ for S1 and $mn = 21$ for S2, are given by

$$ER_{mn} = 10 \log \frac{P_{mn|OFF}}{P_{mn|ON}}. \tag{2}$$

The calculated extinction ratios are shown in Fig. 3(c). In the C-band, the extinction ratio of S1, i.e., ER_{12}, is higher than 15.7 dB (17.9 dB) and that of S2, i.e., ER_{21}, is higher than 17.3 dB (15.7 dB) for the TE (TM) polarization.

The first directional coupler, which is designed for the E_{12} mode, should have little effect on the E_{11} and E_{21} modes propagating in Core 1. Our simulation results show that, in the C-band, the coupling from Core 1 to Core 2 with the E_{11} mode or the E_{21} mode launched into Core 1 is lower than –39 dB, regardless of the state of S1. Similarly, the second directional coupler, which is designed for the E_{21} mode, should have little effect on the E_{11} and E_{12} modes propagating in Core 1. Our simulation results show that, in the C-band, the coupling from Core 1 to Core 2 with the E_{11} mode launched into Core 1 is lower than –36 dB, while that with the E12 mode launched into Core 1 is lower than –28 dB, regardless of the state of S2. These results are polarization-insensitive. The unwanted coupling effects in the two directional couplers are negligible.

2.2 Design II

In Design II, the core dimensions are chosen so that the phase-matching conditions are sufficiently violated when the switches are turned off, but perfect phase matching can be resumed with the switches turned on. The major difference between Design I and Design II is the choice of the widths for Core 2 and Core 3. The dimensions of the two directional couplers are shown in Figs. 4(a) and (b), respectively. The widths of Core 2 and Core 3 are 3.5 and 6.4 μm, respectively, so that the effective indices of the E_{11} modes of Core 2 and Core 3 are sufficiently different from those of the E_{12} and E_{21} modes of Core 1. The phase-matching conditions for this design are shown in Fig. 4(c). With this design, the TO effect is used to activate the directional couplers, i.e., the input high-order mode is coupled to the corresponding output port only when the corresponding switch is turned on. The function of this device is summarized in Fig. 4(d), which is the opposite of that of Design I shown in Fig. 2(d), as far as the functions of the individual TO switches are concerned. The variations of the normalized output light powers with the applied electric power for S1 and S2 at 1550 nm are shown in Figs. 4(e) and (f), respectively. The electric powers required are estimated to be 10.6 and 10.8 mW for S1 and S2, respectively, which are set as the electric powers for the "on" states of the two switches.

The calculated coupling ratios of the fist and the second directional coupler, defined by Eq. (1), are shown in Figs. 5(a) and (b), respectively. In the C-band, $CR_{12|OFF}$ and $CR_{21|OFF}$ are lower than 1.1% (2.5%) and 2.1% (3.2%) for the TE (TM) polarization, respectively, while $CR_{12|ON}$ and $CR_{21|ON}$ are higher than 98.6% (97.5%) and 97.9% (96.8%) for the TE (TM) polarization, respectively.

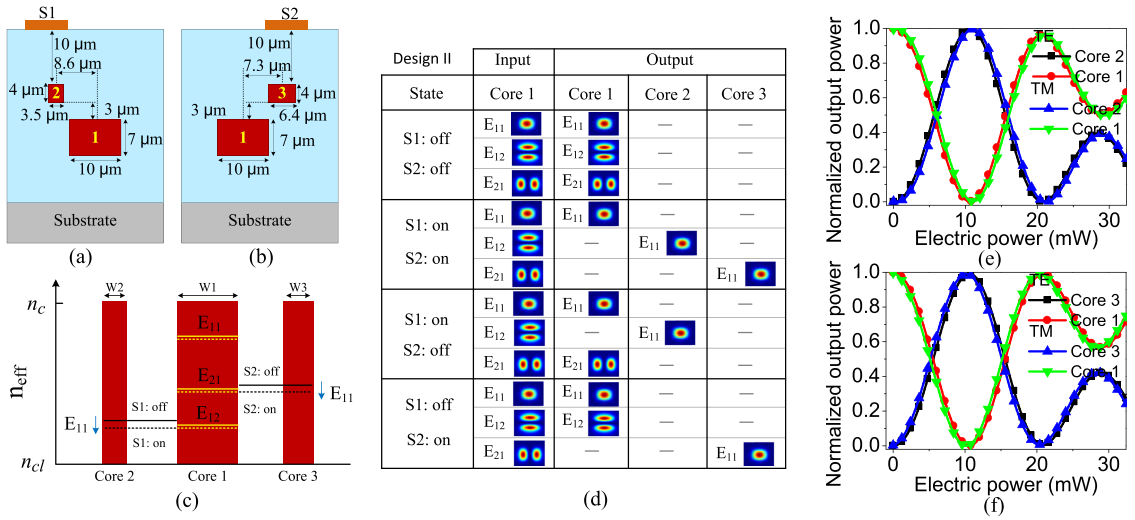

Fig. 4. Design II: dimensions of (a) the first and (b) the second directional coupler; (c) the phase-matching conditions for the two directional couplers, (d) switching functions of the device; and variations of the normalized output powers with the applied electric power for (e) S1 and (f) S2.

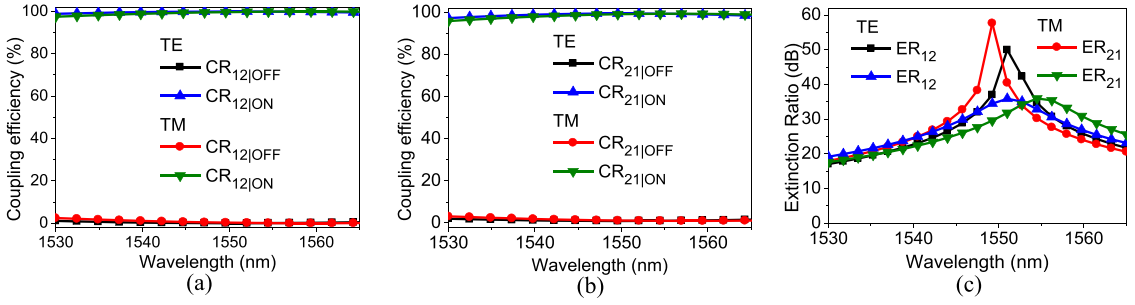

Fig. 5. Design II: coupling ratios for (a) the first and (b) the second directional coupler when the corresponding switches are turned off or on; and (c) the extinction ratios of S1 and S2.

For this design, the extinction ratios of S1 and S2 are given by

$$ER_{mn} = 10 \log \frac{P_{mn|ON}}{P_{mn|OFF}}. \tag{3}$$

The calculated extinction ratios are shown in Fig. 5(c). In the C-band, the extinction ratio of S1, i.e., ER_{12}, is higher than 17.0 dB (17.9 dB) and that of S2, i.e., ER_{21}, is higher than 19.2 dB (17.6 dB) for the TE (TM) polarization.

Again, we can estimate the unwanted coupling effects in the two directional couplers by simulation. In the C-band, the coupling from Core 1 to Core 2 with the E_{11} mode launched into Core 1 is lower than –32 dB, while that with the E_{21} mode launched into Core 1 is lower than –28 dB, regardless of the state of S1. Similarly, in the C-band, the coupling from Core 1 to Core 2 with the E_{11} mode launched into Core 1 is lower than –43 dB, while that with the E_{12} mode launched into Core 1 is lower than –36 dB, regardless of the state of S2. These results are polarization-insensitive.

3. Device Fabrication

We followed the design parameters for Design I and Design II and fabricated the devices with the in-house microfabrication facilities. We used the polymer materials EpoCore and EpoClad (Micro Resist Technology GmbH) as the core and the cladding material, respectively. The refractive

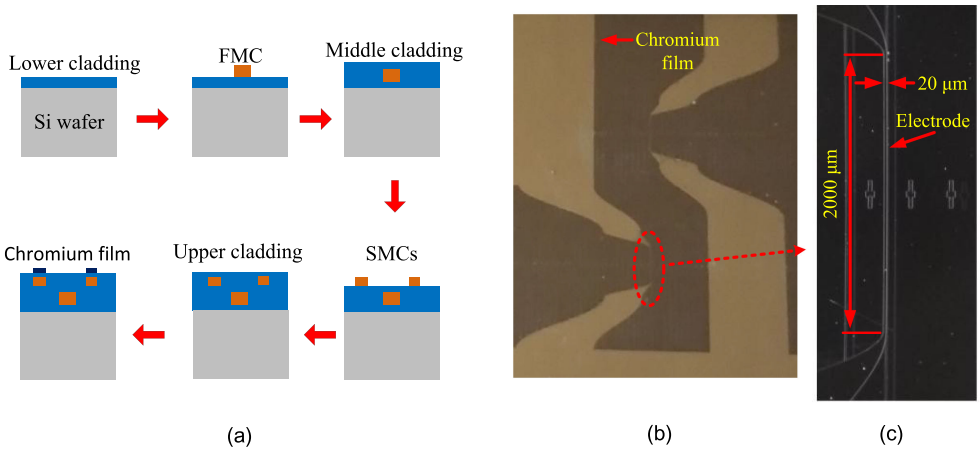

Fig. 6. (a) Steps in the fabrication of the proposed 3D mode spatial switches and photographs of a fabricated device showing (b) the patterned chromium film and (c) one of the electrode heaters.

indices of these two materials, which were measured with a prism coupler (Metricon 2010) on thin-film samples at the wavelength 1536 nm, were 1.569 and 1.559, respectively. The refractive-index difference between the TE and TM polarizations was smaller than 0.001 for both materials. The fabrication process is illustrated in Fig. 6(a) and can be summarized as follows. First, the cladding material is spin-coated onto a silicon substrate to form a sufficiently thick ($>$15 μm) under-cladding. Second, the FMC is formed by spin-coating the core material onto the cured under-cladding and applying photolithography with a mask that defines the core pattern in the lower layer. The height of the core is trimmed to 7.0 μm by reactive-ion etching (RIE) after curing. Third, a middle cladding is spin-coated onto the core layer, which has a thickness of 10.0 μm after curing and RIE trimming. Fourth, SMCs are formed by spin-coating the core material onto the middle cladding and applying photolithography with a mask that defines the core pattern in the upper layer. The heights of all the SMCs are trimmed to 4.0 μm by RIE after curing. Fifth, the cladding material is coated onto the SMCs to form a 14 μm upper-cladding. Finally, a layer of chromium film (about 120 nm) is deposited onto the cured upper-cladding by plasmatic deposition (Desktop Pro, Denton Vacuum) and the electrode heater patterns are defined by photolithography with a mask and a positive photoresist (AZ 5206E). Figure 6(b) shows the patterned chromium film on the surface of a fabricated device and Fig. 6(c) shows an enlarged image of one of the electrode heaters. The width and the length of the electrode heater are about 20 μm and 2.0 mm, respectively. We fabricated a number of devices on the same substrate and the total length of the devices was about 27 mm. In the fabrication process, we made our best effort to control the baking and the curing conditions of the polymer materials to ensure that the refractive indices of the materials and the dimensions of the cores were as uniform as possible, not only within the same layer but also across different layers.

4. Device Characterization

To characterize the performances of the fabricated devices, we launched the E_{11} mode into each core with a pigtailed tunable laser (KEYSIGHT) via a lensed fiber and measured the output powers from different cores with a power meter (Newport 2832-C) via a 40X objective lens. We also captured the output near-field images of the devices with an infrared camera. The measurement results of two typical devices for the two designs are detailed below.

4.1 Design I

Figure 7(a) shows an end face of a typical fabricated device for Design I and Figs. 7(b) and (c) show the output near-field images taken when the E_{11} mode (at 1550 nm) was launched into the

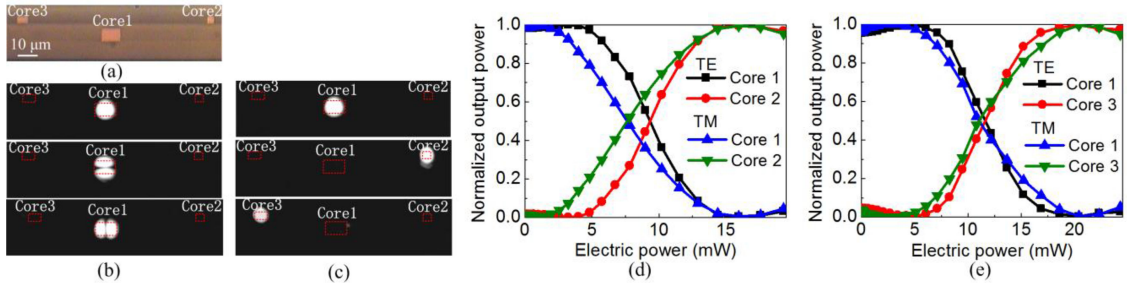

Fig. 7. Design I: (a) photograph of an end face of a fabricated device; near-field images taken at 1550 nm when the E_{11} modes were launched into Core 1, Core 2, and Core 3 (from top to bottom), respectively, with both S1 and S2 turned (b) off or (c) on; and measured variations of the normalized output powers at 1550 nm with the electric power applied to (d) S1 or (e) S2 for the TE and TM polarizations.

three cores, respectively. As shown in Fig. 7(c), when both S1 and S2 are turned off, the E_{11} mode launched into Core 1 stays in Core 1, while the E_{11} modes launched into Core 2 and Core 3 are almost completely coupled to the E_{12} and E_{21} modes of Core 1, respectively. As shown in Fig. 7(c), when both switches are turned on, the E_{11} modes launched into Core 1, Core 2, and Core 3 stay in the original cores. These results confirm the operation of the fabricated device as expected for Design I. Figures 7(d) shows the variations of the normalized output powers from Core 1 and Core 2 with the electric power applied to S1 (while keeping S2 off), when light was launched into Core 2. Figures 7(e) shows the variations of the normalized output powers from Core 1 and Core 3 with the electric power applied to S2 (while keeping S1 off), when light was launched into Core 3. As shown in Figs. 7(d) and (e), the electric powers required for effective switching with S1 and S2 are 15.9 (15.9) and 20.4 (20.6) mW, respectively, for the TE (TM) polarization. Because the distance of Core 2 from Core 1 is larger than that of Core 3 from Core 1, the temperature difference between Core 2 and Core 1 generated by S1 should be higher than that between Core 3 and Core 1 generated by S2 at the same electric power, which explains that the switching power of S1 is lower than that of S2. The butt-coupling losses between the waveguide cores and the lensed fiber are about 1.3, 1.1, and 0.8 dB for Core 1, Core 2, and Core 3, respectively. The propagation losses of the E_{11}, E_{12}, and E_{21} modes along the FMC, measured for a reference FMC of the same dimensions by the cutback method, were ~2.0, ~2.7, and ~2.3 dB/cm at 1550 nm. These losses are insensitive to the wavelength (within the C-band) and the polarization.

By launching the E_{11} mode into Core 2 at the S2 end and measuring the output powers from Core 1 and Core 2 at the S1 end with S1 turned off and on, we were able to evaluate the coupling ratios and the extinction ratios of S1 for the E_{12} mode from Eqs. (1) and (2). Similarly, by launching the E_{11} mode into Core 3 at the S1 end and measuring the output powers from Core 1 and Core 3 at the S2 end with S2 turned off and on, we were able to evaluate the coupling ratios and the extinction ratios of S2 for the E_{21} mode from Eqs. (1) and (2). For the "on" states of S1 and S2, the applied electric powers were set at 15.9 and 20.6 mW, respectively. The measured coupling ratios for the first and the second directional coupler are shown in Figs. 8(a) and (b), respectively. In the C-band, $CR_{12|OFF}$ and $CR_{21|OFF}$ are higher than 96.1% (95.9%) and 97.1% (97.2%) for the TE (TM) polarization, respectively, while $CR_{12|ON}$ and $CR_{21|ON}$ are lower than 2.9% (3.1%) and 4.1% (4.4%) for the TE (TM) polarization, respectively. The measured extinction ratios of S1 and S2 are shown in Fig. 8(c). In the C-band, the extinction ratio of S1, ER_{12}, is higher than 17.1 dB (17.1 dB) and that of S2, ER_{21}, is higher than 16.4 dB (15.6 dB) for the TE (TM) polarization. The wavelength with the highest extinction ratio could be tuned over the range from 1540 to 1560 nm by adjusting the electric power by about ±2 mw. These measurement results compare well with the simulation results shown in Fig. 3 and also confirm that the performance of the device is polarization-insensitive.

To characterize the insertion losses and the crosstalks of the first directional coupler, we launched the E_{11} mode into Core 1, Core 2, and Core 3 at the S2 end with S2 turned off and measured the output powers from the three cores at the S1 end. The transmission spectra, i.e., the output powers

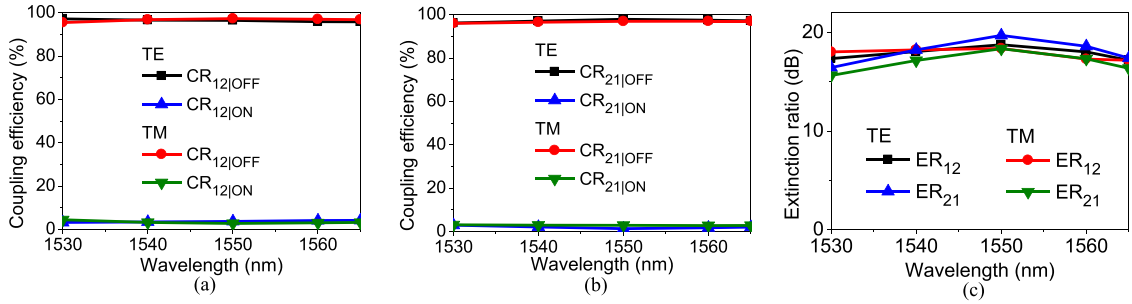

Fig. 8. Design I: coupling ratios (a) $CR_{12|OFF}$ and $CR_{12|ON}$ and (b) $CR_{21|OFF}$ and $CR_{21|ON}$; and (c) extinction ratios ER_{12} and ER_{21}, measured with the electric powers for the "on" states of S1 and S2 fixed at 15.9 and 20.6 mW, respectively.

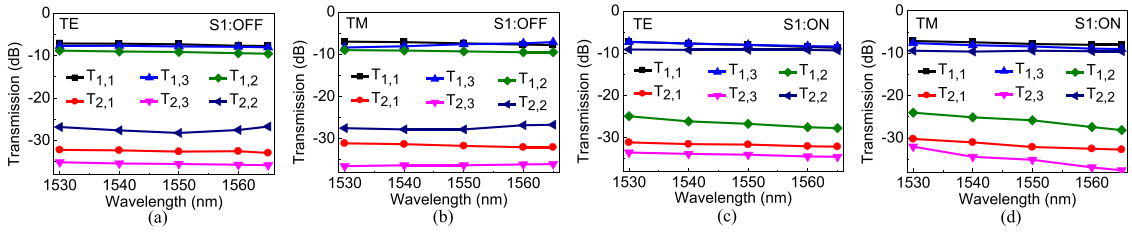

Fig. 9. Design I: transmission characteristics of the first directional coupler for (a) the TE polarization at the "off" state of S1, (b) the TM polarization at the "off" state of S1, (c) the TE polarization at the "on" state of S1, and (d) the TM polarization at the "off" state of S1, measured with S2 turned off.

from Core 1 and Core 2 normalized to the input power launched into the lensed fiber, are shown in Figs. 9(a) and (b) for the "off" state of S1 and in Figs. 9(c) and (d) for the "on" state of S1, where $T_{i,j}$ denotes the transmission from the input Core j ($j = 1, 2, 3$) to the output Core i ($i = 1, 2$) (including the fiber-waveguide coupling loss at the input end). The reason of launching light into Core 3 at the S2 end is to generate a pure E_{12} mode in Core 1 through the second directional coupler (as it is difficult, in practice, to directly excite a pure E_{12} mode from Core 1). At the "off" state of S1, the insertion loss and the crosstalk, given by $T_{1,2}$ and $T_{2,2} - T_{1,2}$, respectively, are lower than 9.5 dB (9.6 dB) and –17.2 dB (–17.1 dB), respectively, in the C-band for the TE (TM) polarization. At the "on" state of S1, the insertion loss and the crosstalk, given by $T_{2,2}$ and $T_{1,2} - T_{2,2}$, respectively, are lower than 9.2 dB (9.1 dB) and –15.8 dB (–15.7 dB), respectively, in the C-band for the TE (TM) polarization. The coupling between the E_{11} modes of Core 1 and Core 2, i.e., $T_{2,1} - T_{1,1}$, is lower than –25.1 dB (–24.1 dB) when S1 is off, or lower than –23.4 dB (–23.1 dB) when S1 is on, for the TE (TM) polarization. The coupling between the E_{21} mode of Core 1 and the E_{11} mode of Core 2, i.e., $T_{2,3} - T_{1,3}$, is lower than –27.4 dB (–28.1 dB) when S1 is off, or lower than –26.1 dB (–24.4 dB) when S1 is on, for the TE (TM) polarization.

Similarly, to characterize the insertion losses and the crosstalks of the second directional coupler, we launched the E_{11} mode into Core 1, Core 2, and Core 3 at the S1 end with S1 turned off and measured the output powers from the three cores at the S2 end. The transmission spectra from various output cores are shown in Figs. 10(a) and (b) for the "off" state of S2 and in Figs. 10(c) and (d) for the "on" state of S2, where $T_{i,j}$ denotes the transmission from the input Core j ($j = 1$, 2, 3) to the output Core i ($i = 1$, 3) (including the fiber-waveguide coupling loss at the input end). The reason of launching light into Core 2 at the S1 end is to generate a pure E_{21} mode in Core 1 through the first directional coupler. At the "off" state of S2, the insertion loss and the crosstalk, given by $T_{1,3}$ and $T_{3,3} - T_{1,3}$, respectively, are lower than 8.5 dB (8.8 dB) and –16.4 dB (–15.6 dB), respectively, in the C-band for the TE (TM) polarization. At the "on" state of S2, the insertion loss and the crosstalk, given by $T_{3,3}$ and $T_{1,3} - T_{3,3}$, respectively, are lower than 8.0 dB (8.3 dB) and –16.4 dB (–16.1 dB), respectively, in the C-band for the TE (TM) polarization. The coupling between the E_{11} modes of Core 1 and Core 3 through the second directional coupler, i.e., $T_{3,1} - T_{1,1}$, is lower

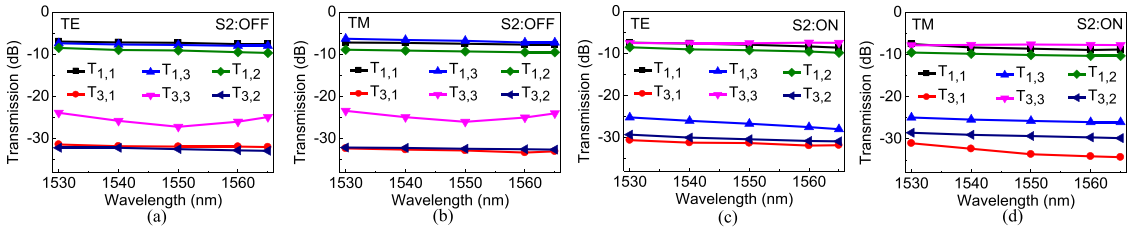

Fig. 10. Design I: transmission characteristics of the second directional coupler for (a) the TE polarization at the "off" state of S2, (b) the TM polarization at the "off" state of S2, (c) the TE polarization at the "on" state of S2, and (d) the TM polarization at the "off" state of S2, measured with S1 turned off.

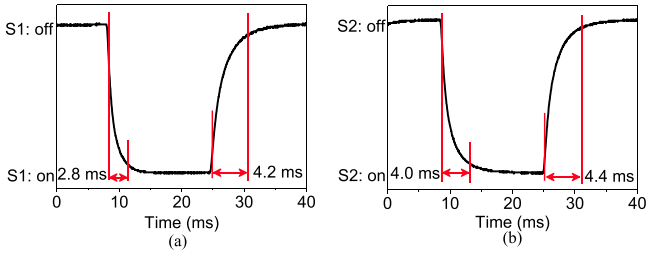

Fig. 11. Design I: temporal response of the device at 1550 nm with (a) S1 or (b) S2 turned on and off periodically with square waves while keeping the other switch off.

than –24.4 dB (–25.1 dB) when S2 is off, or lower than –23.2 dB (–23.5 dB) when S2 is on, for the TE (TM) polarization. The coupling between the E_{12} mode of Core 1 and the E_{11} mode of Core 3, i.e., $T_{3,2} - T_{1,2}$, is lower than –23.2 dB (–23.1 dB) when S2 is off, or lower than –20.8 dB (–21.0 dB) when S2 is on, for the TE (TM) polarization.

As confirmed by these measurement results, the coupling effects for the unintended modes in both directional couplers are small. In other words, the switching of S1 has negligible effects on the output power from Core 3.

To measure the switching speeds of S1, we launched the E_{11} mode into Core 2 and turned S1 on and off periodically with square waves while keeping S2 off. We measured the temporal response of the output optical power from Core1 with a photodetector (Newport 818-IR Detector) and an oscilloscope. The photodetector had a response time shorter than 2 μs. Similarly, to measure the switching speeds of S2, we launched the E_{11} mode into Core 3, turned S2 on and off periodically while keeping S1 off, and measured the temporal response of the output optical power from Core 1. Figures 11(a) and (b) show the output waveforms from Core 1 at 1550 nm displayed on the oscilloscope for the operation of S1 and S2, respectively. For S1, the fall-time and the rise-time are 2.8 and 4.2 ms, respectively, while for S2, the fall-time and the rise-time are 4.0 and 4.4 ms, respectively. The response times are insensitive to the polarization.

4.2 Design II

Figure 12(a) shows an end face of a typical fabricated device for Design II and Figs. 12(b) and (c) show the output near-field images taken when the E_{11} mode (at 1550 nm) was launched into the three cores, respectively. As shown in Fig. 12(b), when both S1 and S2 are turned off, the E_{11} modes launched into Core 1, Core 2, and Core 3 stay in the respective cores. As shown in Fig. 12(c), when both S1 and S2 are turned on, the directional couplers are activated and the E_{11} modes launched into Core 2 and Core 3 are coupled to the E_{12} and E_{21} modes in Core 1, respectively. These results confirm the operation of the fabricated device as expected for Design II. Figure 12(d) shows the variations of the normalized output powers from Core 1 and Core 2 at 1550 nm with the electric power applied to S1 (while keeping S2 off), when light was launched into Core 2. Figure 12(e) shows the variations of the normalized output powers from Core 1 and Core 3

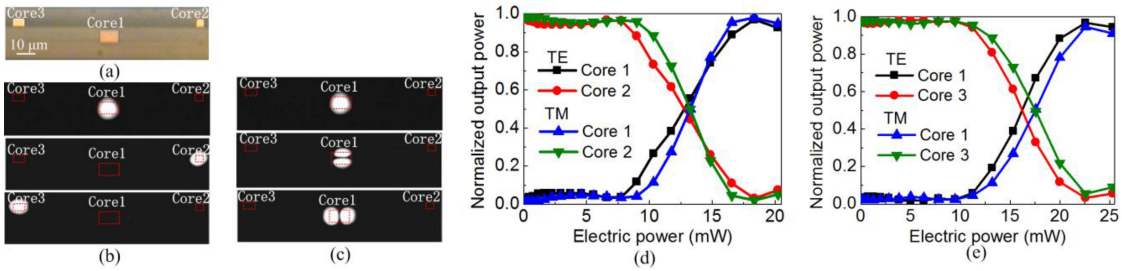

Fig. 12. Design II: (a) photograph of an end face of a fabricated device; near-field images taken at 1550 nm when the E_{11} modes were launched into Core 1, Core 2, and Core 3 (from top to bottom), respectively, with both S1 and S2 turned (b) off or (c) on; and measured variations of the normalized output powers at 1550 nm with the electric power applied to (d) S1 or (e) S2 for the TE and TM polarizations.

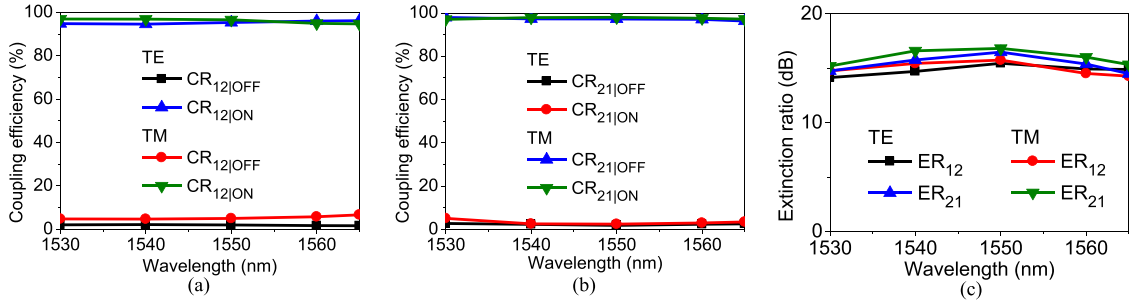

Fig. 13. Design II: coupling ratios (a) $CR_{12|OFF}$ and $CR_{12|ON}$ and (b) $CR_{21|OFF}$ and $CR_{21|ON}$; and (c) extinction ratios ER_{12} and ER_{21}, measured with the electric powers for the "on" states of S1 and S2 fixed at 18.3 and 22.6 mW, respectively.

at 1550 nm with the electric power applied to S2 (while keeping S1 off), when light was launched into Core 3. As shown in Figs. 12(d) and (e), the electric powers required for effective switching with S1 and S2 are 18.3 (18.3) and 22.6 (22.4) mW, respectively, for the TE (TM) polarization. The butt-coupling losses between the waveguide cores and the lensed fiber are about 1.5, 1.1, and 0.9 dB for Core 1, Core 2, and Core 3, respectively, which are similar to those measured for Design I. The mode propagation losses of this device can be taken as the same as those of Design I, as the dimensions of the FMCs in both designs are the same.

We characterized this device in a similar way as for the previous one. To characterize the first directional coupler, we launched the E_{11} mode into Core 1, Core 2, and Core 3 at the S2 end with S2 turned on and measured the output powers from the three cores at the S1 end. To characterize the second directional coupler, we launched the E_{11} mode into Core 1, Core 2, and Core 3 at the S1 end with S1 turned on and measured the output powers from the three cores at the S2 end. For the present device, the "on" states of S1 and S2 correspond to applied electric powers of 18.3 and 22.6 mW, respectively.

The measured coupling ratios for the first and the second directional coupler are shown in Figs. 13(a) and (b), respectively. In the C-band, $CR_{12|OFF}$ and $CR_{21|OFF}$ are lower than 2.2% (6.6%) and 2.7% (5.1%) for the TE (TM) polarization, respectively, while $CR_{12|ON}$ and $CR_{21|ON}$ are higher than 94.5% (94.7%) and 96.2% (97.0%) for the TE (TM) polarization, respectively. The measured extinction ratios of S1 and S2 are shown in Fig. 13(c). In the C-band, the extinction ratio of S1, ER_{12}, is higher than 14.1 dB (15.2 dB) and that of S2, ER_{21}, is higher than 14.5 dB (15.1 dB) for the TE (TM) polarization. These measurement results compare well with the simulation results shown in Fig. 5 and also confirm that the performance of the device is polarization-insensitive.

The transmission characteristics of the first and the second directional coupler are shown in Fig. 14 and Fig. 15, respectively, where $T_{i,j}$ is defined in the same way as for Fig. 9 and Fig. 10. With reference to Fig. 14, for the first directional coupler, the insertion loss and the crosstalk in the

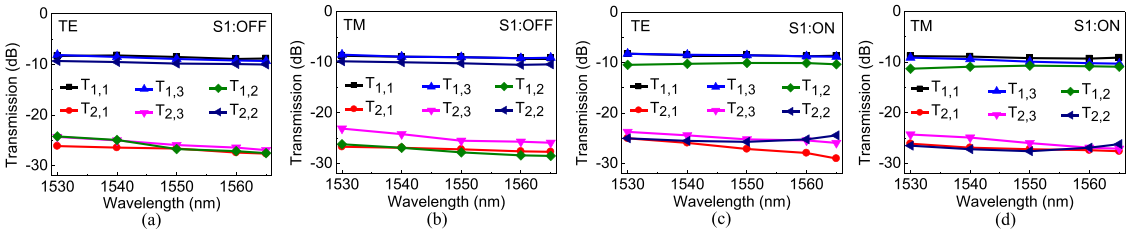

Fig. 14. Design II: transmission characteristics of the first directional coupler for (a) the TE polarization at the "off" state of S1, (b) the TM polarization at the "off" state of S1, (c) the TE polarization at the "on" state of S1, and (d) the TM polarization at the "off" state of S1, measured with S2 turned on.

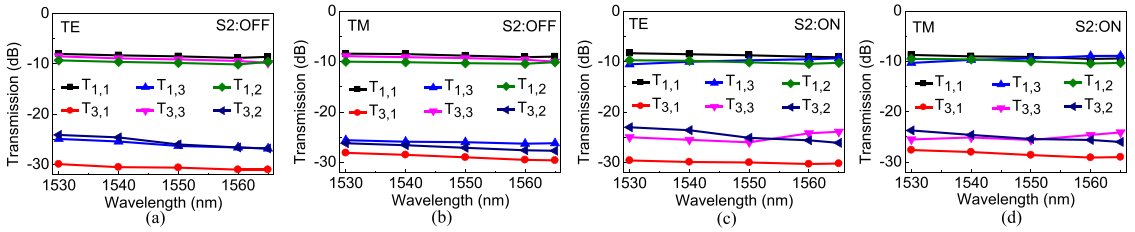

Fig. 15. Design II: transmission characteristics of the second directional coupler for (a) the TE polarization at the "off" state of S2, (b) the TM polarization at the "off" state of S2, (c) the TE polarization at the "on" state of S2, and (d) the TM polarization at the "off" state of S2, measured with S1 turned on.

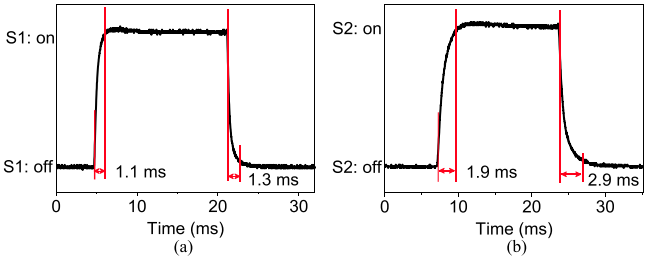

Fig. 16. Design II: temporal response of the device at 1550 nm with (a) S1 or (b) S2 turned on and off periodically with square waves while keeping the other switch off.

C-band at the "off" state of S1, given by $T_{2,2}$ and $T_{1,2} - T_{2,2}$, respectively, are lower than 10.0 dB (10.5 dB) and –14.9 dB (–16.4 dB), respectively, for the TE (TM) polarization, and those at the "on" state of S1, given by $T_{1,2}$ and $T_{2,2} - T_{1,2}$, respectively, are lower than 10.4 dB (11.3 dB) and –14.1 dB (–15.2 dB) for the TE (TM) polarization. The coupling between the E_{11} modes of Core 1 and Core 2, i.e., $T_{2,1} - T_{1,1}$, is lower than –17.8 dB (–18.0 dB) when S1 is off, or lower than –16.8 dB (–17.3 dB) when S1 is on, for the TE (TM) polarization, while the coupling between the E_{21} mode of Core 1 and the E_{11} mode of Core 2, i.e., $T_{2,3} - T_{1,3}$, is lower than –16.2 dB (–16.6 dB) when S1 is off, or lower than –15.8 dB (–15.2 dB) when S1 is on, for the TE (TM) polarization. With reference to Fig. 15, for the second directional coupler, the insertion loss and the crosstalk in the C-band at the "off" state of S2, given by $T_{3,3}$ and $T_{1,3} - T_{3,3}$, respectively, are lower than 9.8 dB (10.0 dB) and –16.4 dB (–16.2 dB), respectively, for the TE (TM) polarization, and those at the "on" state of S2, given by $T_{1,3}$ and $T_{3,3} - T_{1,3}$, respectively, are lower than 10.5 dB (10.3 dB) and –14.5 dB (–15.2 dB), respectively, for the TE (TM) polarization. The coupling between the E_{11} modes of Core 1 and Core 3, i.e., $T_{3,1} - T_{1,1}$, is lower than –21.9 dB (–19.7 dB) when S2 is off, or lower than –20.3 dB (–18.9 dB) when S2 is on, for the TE (TM) polarization, while the coupling between the E_{12} mode of Core 1 and the E_{11} mode of Core 3, i.e., $T_{3,2} - T_{1,2}$, is lower than –14.9 dB (–16.2 dB) when S2 is off, or lower than –15.3 dB (–14.2 dB) when S2 is on, for the TE (TM) polarization. The coupling effects for the unintended modes are small. The switching of S1 has negligible effects on the output power from Core 3.

Figures 16(a) and (b) show the temporal responses for S1 and S2, respectively. For S1, the fall-time and the rise-time are 1.1 and 1.3 ms, respectively, while for S2, the fall-time and the rise-time are 1.9 and 2.9 ms, respectively. The response times are insensitive to the polarization. As the switching powers of Design II are slightly higher than those of Design I, the response times of Design II are also slightly shorter. The response times of our devices are comparable to those of reported TO polymer-waveguide devices [34], [35].

5. Conclusions

We have demonstrated two designs of broadband mode-selective spatial switches based on the configuration of two cascaded TO-controlled vertical directional couplers (Design I and Design II), which differ in the application of the TO effect to deactivate or activate the directional couplers. For Design I, the switching powers of the two TO switches required are 15.9 and 20.6 mW, respectively, and the extinction ratios achieved at these switching powers are higher than 17.1 and 15.6 dB across the C-band, respectively. The switching times are shorter than 4.4 ms. For Design II, the switching powers of the two TO switches required are 18.3 and 22.6 mW, respectively, and the extinction ratios achieved are higher than 14.1 and 14.5 dB across the C-band, respectively. The switching times are shorter than 2.9 ms. The performances of the two devices are weakly sensitive to the polarization state. As shown by our simulation and experimental results, Design I and Design II have comparable performances. The two designs, however, offer different switching functions, as shown in Fig. 2(d) and Fig. 4(d). For energy saving consideration, Design I should preferably be used in situations where spatial separation of the modes in different fibers (the demultiplexing state) is the normal state of the network and only occasional switching to combine modes into the bus fiber (the multiplexing state) is needed. On the other hand, Design II should preferably be used in situations where propagation of all the modes in the bus fiber (the multiplexing state) is the normal state of the network and only occasional switching to add or drop modes from the bus fiber (the demuliplexing state) is needed. Our devices can also function as dynamic power distributors of modes by continuous control of the electric powers applied to the electrode heaters, which could be used, for example, as dynamic mode-dependent loss compensators. It should be possible to further increase the bandwidths of the switches by using tapered directional couplers, but the switching powers required would be higher. Our proposed mode-switching platform has the potential to be exploited for the development of a wide range of active mode-controlling devices for various applications in MDM networks, such as system protection, system testing, system reconfiguration, remote optical provisioning and restoration, etc.

Acknowledgment

The authors would like to thank Mr. Binghui Li for his technical assistance.

References

[1] D. J. Richardson, J. M. Fini, and L. E. Nelson, "Space-division multiplexing in optical fibres," *Nature Photon.*, vol. 7, pp. 354–362, May 2013.
[2] R.-J. Essiambre, G. Kramer, P. J. Winzer, G. J. Foschini, and B. Goebel, "Capacity limits of optical fiber networks," *J. Lightw. Technol.*, vol. 28, no. 4, pp. 662–701, Feb. 2010.
[3] T. Mizuno, H. Takara, A. Sano, and Y. Miyamoto, "Dense space-division multiplexed transmission," *J. Lightw. Technol.*, vol. 34, no. 2, pp. 582–592, Jan. 2016.
[4] T. Mizuno and Y. Miyamoto, "Optical fiber technology high-capacity dense space division multiplexing transmission," *Opt. Fiber Technol.*, vol. 35, pp. 108–117, Feb. 2017.
[5] Y. Ding, J. Xu, F. Da Ros, B. Huang, H. Ou, and C. Peucheret, "On-chip two-mode division multiplexing using tapered directional coupler-based mode multiplexer and demultiplexer," *Opt. Express*, vol. 21, no. 8, pp. 10376–10382, Apr. 2013.
[6] L. Han, S. Liang, H. Zhu, L. Qiao, J. Xu, and W. Wang, "Two-mode de/multiplexer based on multimode interference couplers with a tilted joint as phase shifter," *Opt. Lett.*, vol. 40, no. 4, pp. 518–521, Feb. 2015.
[7] K. Saitoh *et al.*, "PLC-based mode multi/demultiplexers for mode division multiplexing," *Opt. Fiber Technol.*, vol. 35, pp. 80–92, Feb. 2017.

[8] W. Jin and K. S. Chiang, "Three-dimensional long-period waveguide gratings for mode-division-multiplexing applications," *Opt. Express*, vol. 26, no. 12, pp. 15289–15299, Jun. 2018.
[9] A. M. Velazquez-Benitez *et al.*, "Six mode selective fiber optic spatial multiplexer," *Opt. Lett.*, vol. 40, no. 8, pp. 1663–1666, Apr. 2015.
[10] S. H. Chang *et al.*, "All-fiber 6-mode multiplexers based on fiber mode selective couplers," *Opt. Express*, vol. 25, no. 5, pp. 5734–5741, Mar. 2017.
[11] N. Riesen, S. Gross, J. D. Love, and M. J. Withford, "Femtosecond direct-written integrated mode couplers," *Opt. Express*, vol. 22, no. 24, pp. 29855–29861, Dec. 2014.
[12] J. Dong, K. S. Chiang, and W. Jin, "Mode multiplexer based on integrated horizontal and vertical polymer waveguide couplers," *Opt. Lett.*, vol. 40, no. 13, pp. 3125–3128, Jul. 2015.
[13] J. Dong, K. S. Chiang, and W. Jin, "Compact three-dimensional polymer waveguide mode multiplexer," *J. Lightw. Technol.*, vol. 33, no. 22, pp. 4580–4588, Nov. 2015.
[14] T. Watanabe and Y. Kokubun, "Demonstration of mode-evolutional multiplexer for few-mode fibers using stacked polymer waveguide," *IEEE Photon. J.*, vol. 7, no. 6, Dec. 2015, Art. no. 7103311.
[15] Q. Huang, Y. Wu, W. Jin, and K. S. Chiang, "Mode multiplexer with cascaded vertical asymmetric waveguide directional couplers," *J. Lightw. Technol.*, vol. 36, no. 14, pp. 2903–2911, Jul. 2018.
[16] Y. Wu and K. S. Chiang, "Ultra-broadband mode multiplexers based on three-dimensional asymmetric waveguide branches," *Opt. Lett.*, vol. 42, no. 3, pp. 407–410, Feb. 2017.
[17] W. K. Zhao, K. X. Chen, J. Y. Wu, and K. S. Chiang, "Horizontal directional coupler formed with waveguides of different heights for mode-division multiplexing," *IEEE Photon. J.*, vol. 9, no. 5, Oct. 2017, Art. no. 661509.
[18] J. D. Love and N. Riesen, "Mode-selective couplers for few-mode optical fiber networks," *Opt. Lett.*, vol. 37, no. 19, pp. 3990–3992, Oct. 2012.
[19] N. P. Diamantopoulos *et al.*, "Mode-selective optical packet switching in mode-division multiplexing networks," *Opt. Express*, vol. 23, no. 18, pp. 23660–23666, Sep. 2015.
[20] X. Zi, L. Wang, K. Chen, and K. S. Chiang, "Mode-selective switch based on thermo-optic asymmetric directional coupler," *IEEE Photon. Technol. Lett.*, vol. 30, no. 7, pp. 618–621, Apr. 2018.
[21] S. P. Wang, H. Wu, H. K. Tsang, and D. X. Dai, "Monolithically integrated reconfigurable add-drop multiplexer for mode-division-multiplexing systems," *Opt. Lett.*, vol. 41, no. 22, pp. 5298–5301, Nov. 2016.
[22] W. Y. Chan and H. P. Chan, "Reconfigurable two-mode mux/demux device," *Opt. Express*, vol. 22, no. 8, pp. 9282–9290, Apr. 2014.
[23] D. Melati, A. Alippi, and A. Melloni, "Reconfigurable photonic integrated mode (de)multiplexer for SDM fiber transmission," *Opt. Express*, vol. 24, no. 12, pp. 12625–12634, Jun. 2016.
[24] Y. Xiong, R. Priti, and O. Liboiron-Ladouceur, "High-speed two-mode switch for mode-division multiplexing optical networks," *Optica*, vol. 4, no. 9, pp. 1098–1102, Sep. 2017.
[25] B. Stern *et al.*, "On-chip mode-division multiplexing switch," *Optica*, vol. 2, no. 6, pp. 530–535, Jun. 2015.
[26] W. K. Zhao, J. Feng, K. X. Chen, and K. S. Chiang, "Reconfigurable broadband mode (de) multiplexer based on an integrated thermally induced long-period grating and asymmetric Y-junction," *Opt. Lett.*, vol. 43, no. 9, pp. 24–26, May 2018.
[27] Q. Huang, K. S. Chiang, and W. Jin, "Thermo-optic switchable mode multiplexer based on cascaded vertical directional couplers," in *Proc. 2017 Opto-Electron. Commun. Conf. Photon. Global Conf.*, Singapore, 2017, pp. 1–2.
[28] N. Riesen, J. D. Love, and J. W. Arkwright, "Few-mode elliptical-core fiber data transmission," *IEEE Photon. Technol. Lett.*, vol. 24, no. 5, pp. 344–346, Mar. 2012.
[29] F. Parmigiani, Y. Jung, L. Grüner-Nielsen, T. Geisler, P. Petropoulos, and D. J. Richardson, "Elliptical core few mode fibers for multiple-input multiple output-free space division multiplexing transmission," *IEEE Photon. Technol. Lett.*, vol. 29, no. 21, pp. 1764–1767, Nov. 2017.
[30] G. Milione, E. Ip, M. Li, J. Stone, G. Peng, and T. Wang, "Mode crosstalk matrix measurement of a 1 km elliptical core few-mode optical fiber," *Opt. Lett.*, vol. 41, no. 12, pp. 2755–2758, Jun. 2016.
[31] J. Liang, Q. Mo, S. Fu, M. Tang, P. Shum, and D. Liu, "Design and fabrication of elliptical-core few-mode fiber for MIMO-less data transmission," *Opt. Lett.*, vol. 41, no. 13, pp. 3058–3061, Jul. 2016.
[32] X. Sai *et al.*, "Design of elliptical-core mode-selective photonic lanterns with six modes for MIMO-free mode division multiplexing systems," *Opt. Lett.*, vol. 42, no. 21, pp. 4355–4358, Nov. 2017.
[33] Y. Wu and K. S. Chiang, "Mode-selective coupling between few-mode fibers and buried channel waveguides," *Opt. Express*, vol. 24, no. 26, pp. 30108–30123, Dec. 2016.
[34] X. Niu *et al.*, "Thermo-optic waveguide gate switch arrays based on direct UV-written highly fluorinated low-loss photopolymer," *Appl. Opt.*, vol. 53, no. 29, pp. 6698–6705, Oct. 2014.
[35] Z. Cai *et al.*, "Novel fluorinated polycarbonate negative-type photoresists for thermo-optic waveguide gate switch arrays," *J. Mater. Chem. C*, vol. 4, pp. 533–540, Dec. 2015.